Superposed Epoch Analysis of Storm-Time Total Electron Content for the Improvement of Forecast Models

Erik Schmölter and Jens Berdermann

Abstract – The temporal and spatial structures of storm-time ionospheric disturbances are complex and driven by various processes. An understanding of these processes and characterization of the variability are important to validate and improve storm-time ionosphere models, which are, in turn, crucial for reliable operation of communication and navigation services. For that reason, the present study uses a three-step superposed epoch analysis to investigate the temporal and spatial propagation of total electron content enhancements. The results show a distinctive global structure and seasonal variability that is in good agreement with the established understanding of storm-time ionospheric disturbances. Thus, the approach provides a promising tool to validate and improve storm-time ionosphere models.

1. Introduction

Communication and navigation services are impacted by space weather-driven ionospheric disturbances [1, 2]; therefore, ionospheric modeling and forecast are of great interest. For example, geomagnetic storms driven by coronal mass ejections can cause global ionospheric disturbances that propagate in complex structures. For that reason, efforts to develop near real-time forecasts require intensive research and validation to achieve reliable predictions.

The storm-time ionosphere model proposed and developed by [3] predicts the effects of solar storms on the ionospheric total electron content (TEC) on the basis of comparison of real-time and historical solar wind data during events (forecast period of 24 h). The model has been validated with commonly used metrics (e.g., root-mean-square error comparison between observations and predictions) and consequently improved. Nevertheless, differences in the spatial distribution still occur, because the propagation of TEC enhancements is also influenced by other processes (e.g., seasonal variability) [3].

For that reason, the present study investigates the global structure of storm-time TEC in more detail via superposed epoch analysis (SEA). This approach describes changes independent from the specific solar wind conditions and emphasizes other impacts (e.g., seasonal variability). The results may be applied to further validate the storm-time ionosphere model by [3]. The results are also of general interest to better understand storm-time TEC responses.

Manuscript received 13 December 2023.

Erik Schmölter and Jens Berdermann are with the German Aerospace Center, Institute for Solar-Terrestrial Physics, Kalkhorstweg 53, 17235 Neustrelitz, Germany; e-mail: Erik.Schmoelter@dlr.de, Jens.Berdermann@dlr.de.

2. Data

TEC is a commonly used measurement to describe the ionospheric state and its variability. Global TEC maps are provided by the International Global Navigation Satellite System Service (IGS) [4], which were also applied in preceding modeling studies of the storm-time ionosphere [3]. For that reason, rapid high-rate solution TEC maps (15 min cadence) provided on the IGS home page [5] are applied in the present study. A list of approximately 600 historical events (storm onset times at Lagrange point 1) from 1998 to 2018 with significant ionospheric disturbances was established in preceding studies [3] on the basis of literature (e.g., the catalog by [6, 7]) and thresholds for plasma and magnetic field parameters.

3. Method

The present study is primarily concerned with estimating the temporal and spatial propagation of TEC enhancements and applies a three-step SEA approach for that purpose. In short, this requires averaging series of TEC maps with a constant time window starting with the respective storm onset time. However, this general procedure is adapted, as described in the following.

First, TEC maps with grid points according to geographic latitude ϕ and longitude λ are transformed to TEC maps with grid points according to geographic latitude ϕ and local time l. The required shift for this transformation (axis of λ and l) is calculated between the corresponding Universal Time (UT) and 12:00 local time (LT). Thus, the resulting TEC maps are dayside centered and can also be combined without considering the UT storm onset time t_E.

Next, for each onset time t_E from the list of historical events T_E, the TEC maps are extracted from both data sets between $t_E - 3$ h and $t_E + 24$ h. All extracted data sets are stored in a matrix according to time step t, latitude ϕ, longitude λ or local time l, onset time t_E, and day of the year n_d. SEA may be calculated by averaging the data according to dimensions of interest to extract a specific view on the TEC response. Thus, the SEA that is used to emphasize changes according to ϕ and l is calculated as

$$\mathrm{SEA}(t,\phi,l) = \frac{1}{|T_E|}\sum^{|T_E|}\mathrm{TEC}(t_E,t,\phi,l) \tag{1}$$

Two-dimensional representations $\mathrm{SEA}(t,\phi)$ and $\mathrm{SEA}(t,l)$ could be calculated as well, but neither would allow describing the propagation of disturbances. For that

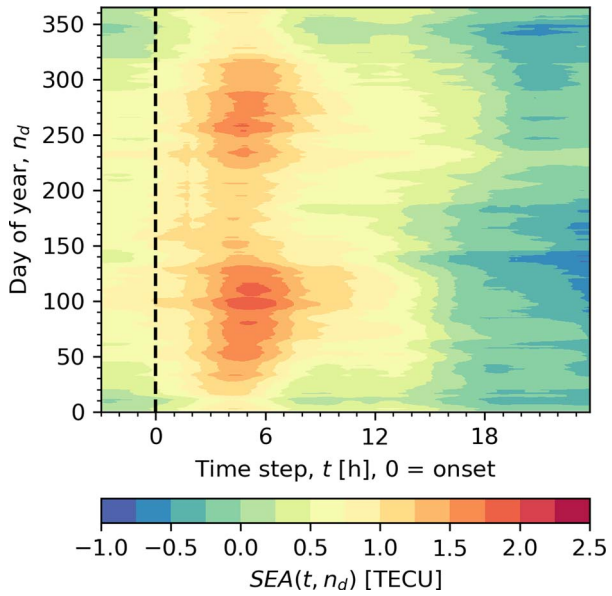

Figure 1. Superposed epoch analysis $\mathrm{SEA}(t, n_d)$ of TEC according to time step t and day of year n_d from onset time t_E. The results are calculated with all entries from the list of historical events. The dashed line marks the storm onset time.

reason, $\mathrm{SEA}(t, \phi, l)$ is instead reduced by estimating the time step $t_{\max}$ of the maximum TEC enhancement as

$$t_{\max}(\phi, l) = \arg\max \mathrm{SEA}(t, \phi, l) \tag{2}$$

The values of the resulting $t_{\max}(\phi, l)$ are time steps (from 0 h to 24 h). The maximum TEC enhancement $\mathrm{TEC}_{\max}$ is similarly calculated as

$$\mathrm{TEC}_{\max}(\phi, l) = \max \mathrm{SEA}(t, \phi, l) \tag{3}$$

4. Results

Figure 1 shows the superposed epoch analysis $\mathrm{SEA}(t, n_d)$ of TEC according to time step t and day of year n_d of the storm onset, with a significant response to the selected events (maximum enhancement at approximately 5 h) and seasonal variability. This result, among others, confirms that the list of event onset times is appropriate to describe storm-time TEC responses. This was established with analysis of selected events [3]. On further analysis, (2) is adjusted to account for this seasonal variability, and two separate periods are analyzed, winter (from December 1 to February 28) and summer (from June 1 to August 31) according to the Northern Hemisphere, with 91 and 75 historical events, respectively (only periods without significant data gaps). Spring and fall would also be of interest, as they show the strongest TEC enhancements (see Figure 1), but much stronger spatial variations are expected between winter and summer.

Figure 2 shows the maximum enhancement time $t_{\max}$ (2) during the Northern Hemisphere winter (a) and summer (b). For both periods, a temporal structure is observed, but transitions between adjacent grid points are especially well defined during the Northern Hemisphere winter. The results presented in Figure 2 describe the temporal structure of the TEC enhancements appropriately. In both periods, TEC enhancements occur first at the poles and propagate toward high latitudes at nightside and 1 h to 2 h later at dayside. Next, the TEC enhancements propagate toward middle latitudes at dayside, and from there, toward nightside ($t_{\max}$ from 3 h to 9 h). The enhancements on both hemispheres merge in low latitudes at nightside and propagate further along the equator ($t_{\max}$ from 9 h to 15 h). The latest enhancements occur at dayside (dawn, 18:00 LT) in Figure 2a and back at nightside (night, 03:00 LT) in Figure 2b. The transition at low latitudes in Figure 2b is interrupted due to stronger TEC enhancements at later $t_{\max}$. Nevertheless, a transition region can be assumed.

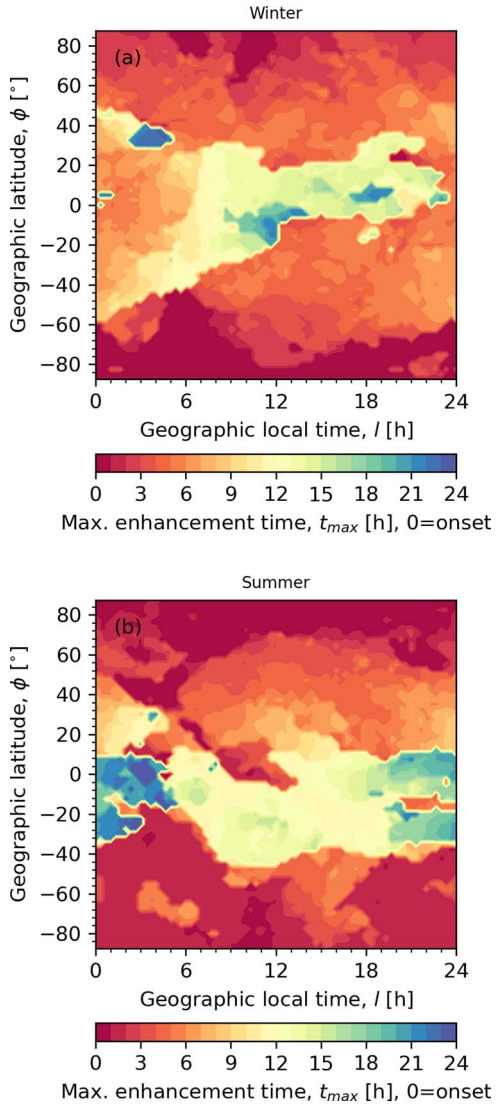

Figure 2. Maximum enhancement time $t_{\max}$ according to geographic local time l and latitude ϕ during Northern Hemisphere winter (a) and summer (b).

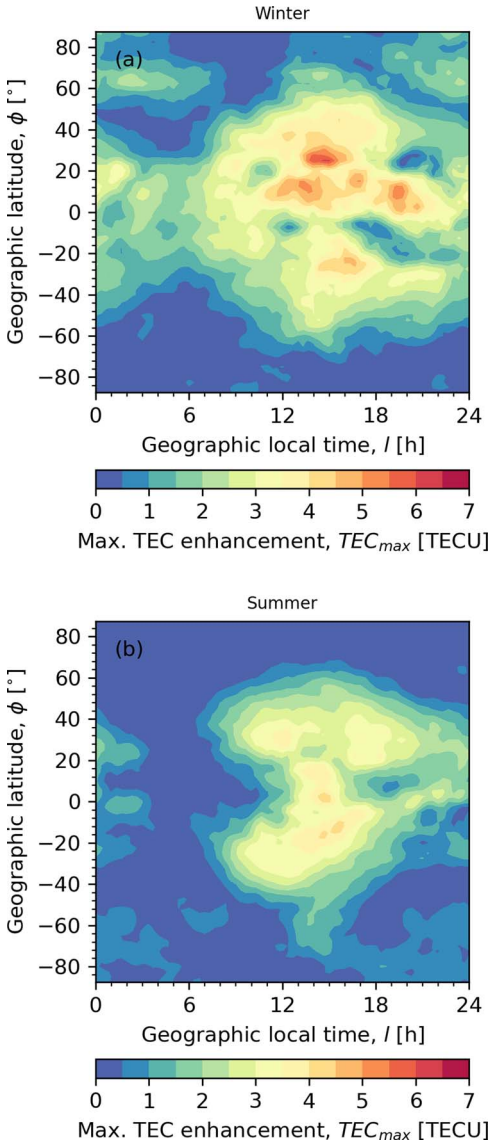

Figure 3. Maximum TEC enhancement TEC_{max} according to geographic local time l and latitude ϕ during Northern Hemisphere winter (a) and summer (b).

Further, the global structure is shifted by approximately 10° northward in Figure 2a and southward in Figure 2b. Thus, various differences are observed due to seasonal variability. Generally, the results are in good agreement with the established understanding of storm-time TEC [8, 9].

The maximum TEC enhancement TEC_{max} (3) is shown in Figure 3 according to t_{max} in Figure 2. The global structures of t_{max} and TEC_{max} are moderately correlated (correlation coefficient of 0.45), and, for example, in the initial period, a similar increase from high to middle latitudes occurs (correlation coefficient of 0.65 at t_{max} from 0 h to 6 h). During the transition from middle to low latitudes, the correlation decreases (correlation coefficient of 0.25 at t_{max} from 6 h to 14 h), because TEC_{max} is decreased on the nightside. Thus, an

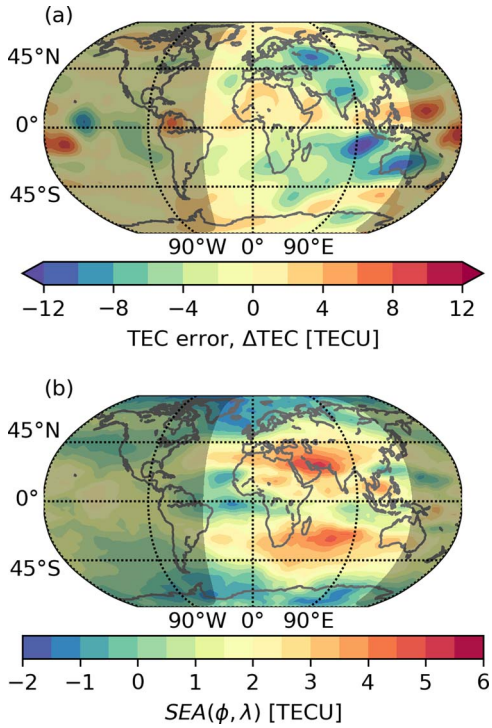

Figure 4. Difference between observed and predicted TEC during Saint Patrick's Day geomagnetic storm at March 17, 2015 (6 h after onset) according to the forecast model by [3] (a) and superposed epoch analysis $SEA(\phi, \lambda)$ of TEC for the corresponding day of year and time step (b). The nightside is indicated with dark shading.

analysis on the basis of only TEC_{max} cannot indicate the relation with geographic local time.

5. Discussion

Figure 4a shows an example of a TEC error map from the forecast model by [3] during the Saint Patrick's Day geomagnetic storm on March 17, 2015. Large structures with negative values at low and middle latitudes are observed for the dayside. Smaller structures with positive or negative values are observed for the nightside. These features are weakly correlated to the $SEA(\phi, \lambda)$ for this day of the year and time step (see Figure 4b). These results are calculated by transforming the $SEA(\phi, l)$ from geographic local time to longitude according to the onset time of the Saint Patrick's Day geomagnetic storm. If the correlation exists for other events as well, then the SEA results may be applied for regional adjustments according to Figure 2. If, for example, the SEA result in Figure 4b is simply added to corresponding predictions of the example TEC error map in Figure 4a, then the reported root mean square error of 3.22 TECU [3] is reduced to 2.90 TECU.

The proposed approach could be improved, because more pronounced transitions are preferable. In particular, the results in Figure 2b show more small-scale variations and are, therefore, more difficult to analyze. This is partly due to the smaller number of available reference events, which, however, will increase as solar cycle 25 progresses. A more challenging problem is the superposition of TEC

enhancements along the equator in Figure 2b. This problem may be solved by identifying secondary maxima to analyze these regions in more detail. Generally, the approach would also benefit from a higher spatial and temporal resolution.

6. Conclusion

The present study applied a three-step SEA approach to investigate the temporal and spatial propagation of TEC enhancements during storm times. The matrix calculated for this purpose allows us to describe these TEC responses according to day of the year or UT onset time. More categories could be added (e.g., geomagnetic activity level) using the list of historical events. The calculated TEC response according to geographic latitude and local time (see Figure 2) is in good agreement with other studies [8, 9] and provides well-defined structures for the maximum TEC enhancements.

For that reason, the forecasts of the storm-time ionosphere model by [3] will be analyzed with the new results. Of particular interest is whether previously identified spatial deviations occur in cases in which the predicted temporal and spatial propagation of TEC enhancements differ from the SEA results. If such a correlation is found, these deviations can be minimized using the SEA approach. If not, the investigated processes can be considered of lower importance in further analyses. Either way, the new results provide more insight into storm-time TEC responses.

7. Acknowledgment

We thank the International Global Navigation Satellite System Service for providing rapid high-rate solution total electron content maps via the Crustal Dynamics Data Information System Web interface [5].

8. References

1. B. Arbesser-Rastburg and N. Jakowski, “Effects on Satellite Navigation,” in V. Bothmer and I. A. Daglis(eds.), *Space Weather: Physics and Effects*, Berlin, Springer, 2007, Chapter 13.
2. L. J. Lanzerotti, “Space Weather Effects on Communications,” in V. Bothmer, and I. A. Daglis(eds.), *Space Weather: Physics and Effects*, Berlin, Springer, 2007, Chapter 9.
3. E. Schmölter and J. Berdermann, “Predicting the Effects of Solar Storms on the Ionosphere Based on a Comparison of Real-Time Solar Wind Data With the Best-Fitting Historical Storm Event,” *Atmosphere*, **12**, 12, December 2021, p. 1684.
4. M. Hernández-Pajares, J. M. Juan, J. Sanz, R. Orus, A. Garcia-Rigo, et al., “The IGS VTEC Maps: A Reliable Source of Ionospheric Information Since 1998,” *Journal of Geodesy*, **83**, February 2009, pp. 263–275.
5. Crustal Dynamics Data Information System, “GNSS Atmospheric Products: Ionosphere,” https://cddis.nasa.gov/archive/gnss/products/ionex/ (Accessed 14 February 2024).
6. H. V. Cane and I. G. Richardson, “Interplanetary Coronal Mass Ejections in the Near-Earth Solar Wind During 1996–2002,” *Journal of Geophysical Research: Space Physics*, **108**, A4, April 2003, p. 1156.
7. I. G. Richardson and H. V. Cane, “Near-Earth Interplanetary Coronal Mass Ejections During Solar Cycle 23 (1996–2009): Catalog and Summary of Properties,” *Solar Physics*, **264**, 1, May 2010, pp. 189-237.
8. S. M. Stankov, K. Stegen, and R. Warnant, “Seasonal Variations of Storm-Time TEC at European Middle Latitudes,” *Advances in Space Research*, **46**, 10, November 2010, pp. 1318-1325.
9. S. J. Adebiyi, I. A. Adimula, and O. A. Oladipo, “Seasonal Variations of GPS Derived TEC at Three Different Latitudes of the Southern Hemisphere During Geomagnetic Storms,” *Advances in Space Research*, **53**, 8, April 2014, pp. 1246-1254.